Effects of a local auxiliary protein on the two-dimensional affinity of a TCR-peptide MHC interaction

Victoria Junghans[1], Manto Chouliara[1], Ana Mafalda Santos[2], Deborah Hatherley[2], Jan Petersen[4], Tommy Dam[1], Lena M. Svensson[3], Jamie Rossjohn[4,5], Simon J. Davis[2], Peter Jönsson[1*]*

[1]Department of Chemistry, Lund University, Lund, Sweden

[2]Radcliffe Department of Medicine, John Radcliffe Hospital, University of Oxford; and Medical Research Council Human Immunology Unit, John Radcliffe Hospital, University of Oxford, OX3 9DS Oxford, UK.

[3]Department of Experimental Medical Science, Lund University, Lund, Sweden; and School of Medical Sciences, Örebro University, Örebro, Sweden

[4]Infection and Immunity Program & Department of Biochemistry and Molecular Biology, Biomedicine Discovery Institute, Monash University, Clayton, Victoria 3800, Australia; and Australian Research Council Centre of Excellence in Advanced Molecular Imaging, Monash University, Clayton, Victoria 3800, Australia.

[5]Institute of Infection and Immunity, Cardiff University School of Medicine, Heath Park, Cardiff CF14 4XN, UK.

*** Correspondence:**

Peter Jönsson

peter.jönsson@fkem1.lu.se

Victoria Junghans

victoria.junghans@fkem1.lu.se

Keywords: T-cell receptor, major histocompatibility complex, affinity, protein binding, CD2, lamellipodia

Summary: Two-dimensional affinity measurements of a T-cell receptor binding its agonistic peptide major histocompatibility complex molecule and the influence of cellular context.

Abstract

The affinity of T-cell receptors (TCRs) for major histocompatibility complex molecules (MHCs) presenting cognate antigens likely determines whether T cells initiate immune responses, or not. There exist few measurements of two-dimensional (2D) TCR-MHC interactions, and the effect of auxiliary proteins on binding is unexplored. Here, Jurkat T-cells expressing the MHC molecule HLA-DQ8-glia-α1 and the ligand of an adhesion protein (rat CD2) were allowed to bind supported lipid bilayers (SLBs) presenting fluorescently-labelled L3-12 TCR and rat CD2, allowing measurements of binding unconfounded by cell signaling effects or co-receptor binding. The 2D K_d for L3-12 TCR binding to HLA-DQ8-glia-α1, 14±5 molecules/μm^2, was only marginally influenced by including CD2 up to ~200 bound molecules/μm^2 but higher CD2 densities reduced the affinity up to 1.9-fold. Cell-SLB contact size increased steadily with ligand density without affecting binding for contacts up to ~20% of total cell area but beyond this lamellipodia appeared, giving an apparent increase in bound receptors of up to 50%. Our findings show how parameters other than the specific protein-protein interaction can influence binding behavior at cell-cell contacts.

Introduction

The interaction between T-cell receptors (TCRs) and different peptide-presenting major histocompatibility complex molecules (MHCs) is vital for the response of T lymphocytes in the adaptive immune system. It both decides whether the T lymphocyte should undergo positive and negative selection in the thymus as well as being the initial step in triggering a T-cell response against foreign pathogen (van der Merwe and Dushek, 2011). The affinity of the TCR-MHC interaction has been considered to be an important factor in how the T cell responds in these settings, and has been observed to correlate with T-cell signaling potency (Huang et al., 2010; Huppa et al., 2010). However, it is to date not understood how the TCR can distinguish between activating and non-activating ligands (Chakraborty and Weiss, 2014; Dustin et al., 2001; Morris and Allen, 2012). To understand this further, various techniques have been developed to study the relatively weak interactions of TCRs with ligand-presenting MHCs. Surface plasmon resonance was one of the first techniques used to measure the interaction of soluble TCRs to immobilized MHCs generating three-dimensional (3D) dissociation constants (K_d) (Garcia et al., 1997; Matsui et al., 1994). A vast diversity of TCRs and MHCs have since been investigated ranging from agonistic (1-200 μM) to antagonistic interactions (> 5 μM) (Alam et al., 1999; Rosette et al., 2001; Rossjohn et al., 2015; Stone et al., 2009; Sumen et al., 2004). However, 3D K_ds can differ substantially from binding affinities in a cell-cell contact, where both receptors and ligands are laterally confined in two dimensions (2D) and are affected by cellular dynamics and protein flexibility (Hu et al., 2013; Huang et al., 2010; Huppa et al., 2010; Xu et al., 2015). Unfortunately, measuring 2D K_ds is considerably less common, and more difficult, than performing 3D affinity measurements. The number of measured 2D K_ds of TCR-MHC interactions is therefore limited (Dustin et al., 1997; Grakoui et al., 1999; Huang et al., 2010; Huppa et al., 2010; Zhu et al., 2007; Zhu et al., 2013), hampering the development of new theories to explain T-cell signaling and antigen discrimination. Furthermore, there are multiple different types of molecules binding across the cell-cell contacts *in vivo* that can influence the binding behavior in the contact. Auxiliary binding molecules have previously been used in 2D K_d measurements to ensure contact formation and to promote bond formation between weaker-binding ligands and their receptors (Grakoui et al., 1999; Jönsson et al., 2016). However, it is not well known how and if this affects the 2D K_d of the studied system (Grakoui et al., 1999; Jönsson et al., 2016; O'Donoghue et al., 2013).

The aim of the present study was to investigate how the 2D K_d of a prototypical TRBV9$^+$ TCR (L3-12) binding to its agonist MHC class II molecule, the human leukocyte antigen protein DQ8 presenting the α-1 gliadin peptide (HLA-DQ8-glia-α1), depends on cellular context and

in particular how this interaction is influenced by auxiliary binding molecules in the cell contact. HLA-DQ8-glia-α1 is known to be associated with celiac disease, a T-cell mediated autoimmune-like disorder characterized by repeated patterns of TRBV9^{+} TCR usage against an immunodominant α-1 gliadin determinant (Broughton et al., 2012). The L3-12 TCR has a higher solution affinity (7 μM) (Broughton et al., 2012) than typically observed for microbial and non-self peptide-presenting MHC class II molecules (~30 μM) (Cole et al., 2007) and binds considerably more strongly than autoreactive TCR-MHC complexes (100-200 μM) (Bulek et al., 2012; Deng and Mariuzza, 2007). However, a 2D K_d value for this interaction has not been determined.

Rat CD2 (rCD2) binding the rat CD48 mutant T92A (rCD48$_{T92A}$) was used as the auxiliary binding pair in this study. The rCD2-rCD48$_{T92A}$ interaction has a 3D K_d of 11 μM which is comparable to that of the human adhesion pair CD2-CD58 (Evans et al., 2006). Both HLA-DQ8-glia-α1 and rCD48$_{T92A}$ were expressed in Jurkat T cells that do not naturally express these receptors and the cells were allowed to bind to supported lipid bilayers (SLBs) with different amounts of fluorescently-labelled L3-12 TCR and rCD2 ligands. By using this model system three sources of confounding effects were avoided: (i) the effects of T-cell activation on receptor reorganization and binding (Limozin et al., 2019; Zhu et al., 2006), allowing us to focus on the conditions prior to T-cell signaling; (ii) the influence co-receptor binding can have on the TCR-MHC 2D K_d, which could distort the measurement; and (iii) the budding off of TCR-enriched microvesicles into the contact (Choudhuri et al., 2014), which would result in an underestimation of the true 2D K_d value by the Zhu-Golan method. By removing these effects from the experiments, we could focus on the direct influence that auxiliary molecules and cellular context have on the TCR-MHC 2D K_d.

The 2D K_d of the interaction was obtained by relating the accumulation of the ligands at different initial ligand densities at the SLB using the Zhu-Golan expression (Zhu et al., 2007):

$$\frac{B}{F} = \frac{N_{\mathrm{tot}} \times f}{K_{\mathrm{d}} \times S_{\mathrm{cell}}} - \frac{B \times p}{K_{\mathrm{d}}} \qquad \textbf{(1)}$$

where B and F are the bound and free density of the ligands, $N_{tot} \times f$ the total number of mobile counter-receptors on the cell, S_{cell} is the total cell surface area and p the ratio of the cell-SLB contact area to S_{cell}. Measurements were initially made for the L3-12 TCR binding HLA-DQ8-glia-α1 and rCD2 binding rCD48$_{T92A}$ alone and then in the presence of the auxiliary protein rCD2 or L3-12 TCR, respectively. At high densities of the auxiliary protein the 2D K_d of the studied ligand decreased almost twofold. It was also observed that cell-SLB contact sizes increased linearly with the amount of bound ligands but affected ligand binding behavior only

at larger contacts characterized by lamellipodium formation. This altogether suggests that there is not a single parameter determining the 2D K_d of a ligand-receptor interaction and that it is important to understand these effects and the cellular context in which the measurements are done to obtain more reproducible 2D K_d values experimentally as well as to better understand how these proteins bind and mediate their functions *in vivo*.

Results

The 2D K_d of the L3-12 TCR binding HLA-DQ8-glia-α1

Jurkat T cells expressing HLA-DQ8-glia-α1 were allowed to attach to an SLB presenting fluorescently-labelled L3-12 TCR (**Figure 1A**). The L3-12 TCR bound to HLA-DQ8-glia-α1 on the cells and accumulated beneath the cells visibly as an increase in fluorescence intensity (**Figure 1B**). This fluorescence intensity can be converted to the total sum of ligands in the contact (bound and free, $B + F$). The intensity outside the contact gives the free ligand density in the contact (F), after multiplication with a correction factor to take into account the exclusion of free ligands in the contact (see Materials and Methods for details). The subsequent addition of more TCR to the same SLB resulted in a shift in F and B, corresponding to higher free ligand densities and more bound receptors. The changes in B, F and p were plotted in a Zhu-Golan plot as defined by **Eqn. 1** (**Figure 1C**). It was confirmed that using SLBs with multiple additions of ligands did not influence the profile of the Zhu-Golan curve compared to when different SLBs were used for the studied concentrations (**Figure S1**). The ratio of bound vs free ligands decreased with an increasing number of added ligands. However, at high ligand densities, typically when the contact-to-surface area ratio p was above 0.2, the Zhu-Golan plot started levelling off with only minor changes in B/F. This effect will be discussed below. For Figure 2, only ligand density data points below $B \times p = 300$ molecules/μm^2 are included where these effects are non-significant. The Zhu-Golan data points here follow Eqn. 1 and fitting the data gave a 2D K_d of 14±5 molecules/μm^2. This value is in the range of previously measured 2D K_d values of TCR-agonist MHCs (10 – 110 molecules/μm^2) (Grakoui et al., 1999; Huppa et al., 2010; Pielak et al., 2017).

The total amount of mobile HLA-DQ8-glia-α1 molecules on the cells was $N_{tot} \times f = 405\,000 \pm 108\,000$ which was obtained from the x-intersect in the Zhu-Golan plot using an average S_{cell} of 700 μm^2 assessed from the cell diameter observed using widefield microscopy. With the mobile fraction of the receptors being $f = 0.9 \pm 0.1$ (**Movie S1 and S2**), measured using fluorescence recovery after photobleaching (FRAP), this corresponds to a total amount of,

mobile and immobile, HLA-DQ8-glia-α1 molecules per cell of N_{tot} = 450 000±120 000 molecules. This value is within the experimental error identical to the value measured by flow cytometry (**Table 1**). Previously, it has been shown that the total receptor number on the cells, N_{tot}, obtained from the Zhu-Golan curves can be higher than the total number of receptors measured using antibody binding (Dustin et al., 1997; Zhu et al., 2007). This effect was accounted for by a greater tendency of cells expressing larger numbers of receptors to bind to the SLB biasing the measured total amount of receptors using the Zhu-Golan analysis towards larger N_{tot} values (Dustin et al., 1997; Zhu et al., 2007). Since our measured N_{tot} is the same as that obtained from flow cytometry, we conclude that under the experimental conditions used here there was no significant bias towards cells expressing larger numbers of receptors binding to the SLB.

The affinity of rCD2 binding rCD48$_{T92A}$

Measurements of rCD2 binding to rCD48$_{T92A}$ expressed on Jurkat T cells were also performed. First, Jurkat T cells expressing rCD48$_{T92A}$ were added to a rCD2-functionalized SLB resulting in the accumulation of rCD2 underneath the cell. More rCD2 was added and the obtained data fitted to the Zhu-Golan expression in **Eqn. 1** (**Figure 1D**). The 2D K_d was subsequently found to be 6±1 molecules/μm^2, with the total amount of rCD48$_{T92A}$ molecules on the cell N_{tot} = 124 000±9 000 molecules, and f = 0.6±0.2 measured separately by FRAP (**Movie S3 and S4**). The total amount of rCD48$_{T92A}$ molecules on the cell was, as for HLA-DQ8-glia-α1, within the accuracy of the experiment identical to the number measured by flow cytometry (**Table 1**). The 2D K_d value is approximately seven-fold lower than that of rCD2 binding wild type rCD48, measured under otherwise similar conditions to those used in this work (Jönsson et al., 2016). This is a larger relative difference compared to the corresponding change in 3D affinity between the T92A mutant and the wildtype CD48 (3-4-fold) (Evans et al., 2006). The 2D affinity for rCD2 binding rCD48$_{T92A}$ is furthermore similar in magnitude to that measured previously for human CD2 binding human CD58 (Tolentino et al., 2008; Zhu et al., 2007).

Binding affinities are not affected by the presence of another ligand at low densities

To investigate whether having two different binding ligands influences the affinities of each other, SLBs containing both rCD2 and L3-12 TCR were next studied. This was done at either low or high concentrations of the additional ligand. In all cases the proteins, rCD2 and L3-12 TCR, bound to the Jurkat T cells and distributed homogeneously within the cell contact area (**Figure 2A and B**). Having rCD2 at densities below B_{rCD2} = 200 molecules/μm^2 (low densities)

had no significant effect on the 2D K_d of the L3-12 TCR binding HLA-DQ8-glia-α1 interaction (**Figure 2C, Figure S2**). However, increasing the densities of bound rCD2 to above 300 molecules/μm^2 (high densities) increased the effective 2D K_d by a factor of 1.9 to 26±1 molecules/μm^2 (**Figure 2D**). The limits for the low and high densities of rCD2 were chosen empirically and are different to when L3-12 TCR and HLA-DQ8-glia-α1 were considered as the auxiliary binding pair (see below). Additionally, the maximum amount of bound L3-12 TCR was reduced by 37% compared to L3-12 TCR binding in the absence of rCD2 (**Figure S2**). A similar effect was observed when adding the L3-12 TCR as an auxiliary ligand to rCD2-functionalized SLBs. At densities of L3-12 TCR below B_{TCR} = 700 molecules/μm^2 the rCD2 binding rCD48$_{T92A}$ interaction was only moderately affected (**Figure 2E**), whereas at densities above 900 molecules/μm^2 of bound L3-12 TCR the Zhu-Golan plot for rCD2 binding rCD48$_{T92A}$ shifted downward, resulting in a 1.5 fold larger 2D K_d of 9±1 molecules/μm^2 (**Figure 2F**). Moreover, in the latter case, the maximum amount of bound rCD2 in the contact decreased by 43% (**Figure S2**). The Zhu-Golan plots levelled off at high ligand concentrations for both protein pairs, which occurred at $B \times p$ > 300 molecules/μm^2 for L3-12 TCR binding HLA-DQ8-glia-α1 and at $B \times p$ > 100 molecules/μm^2 for rCD2 binding rCD48$_{T92A}$. These data points were excluded from Figure 2 and will be discussed below. A contributing factor to the increase in the 2D K_d values at high densities of auxiliary molecules could be that the auxiliary molecules aid in excluding free ligands and receptors from the cell contact, thereby lowering the effective affinity. Another possible explanation for the increased 2D K_d could be competition between the two ligands in forming receptor-ligand contacts, resulting in a lower on-rate and/or lifetime of the individual interaction thereby lowering the affinity. Both these effects could arise if there is a height mismatch between the two ligand-receptor pairs (Milstein et al., 2008; Weikl et al., 2019). Another influencing factor could be crowding due to the addition of a second ligand, however, from previous measurements of the lateral interactions between rCD2 molecules in an SLB (Junghans et al., 2018), it is unlikely that this would be a significant effect at the concentrations used here. Of note, the observed decrease in the amounts of bound ligands when adding auxiliary molecules also depended on the cell-SLB contact size. Contact area was in general larger when having auxiliary molecules (**Figure 3**), thus reducing the receptor density in the contact resulting in smaller amounts of bound molecules.

Increased contact area formation with ligand density

Contact formation occurred at ligand densities above F = 20 molecules/μm^2 for both L3-12 TCR and for rCD2. The bound cells at these ligand densities appeared spherical in the widefield

images (**Figure 3A**). Increasing the ligand densities led to cell spreading on the bilayer and a contact size that increased approximately linearly with the number of bound receptors ($B \times p$) (**Figure 3**). A similar linear trend has previously been noted by Shao *et al*. (Shao et al., 2005). Cell deformations have been observed for T cells interacting with B cells which was suggested to play a crucial role in T-cell activation (Negulescu et al., 1996). In the presence of both the L3-12 TCR and rCD2 the contact area was generally larger as compared to the cell contact when there was only one protein species on the SLB (**Figure 3B and C**). This effect was especially noticeable at higher ligand densities (see values above $p_{lam} = 0.2$ in **Figure 3B and C)**. However, the average contact size in these experiments did not grow larger than 40% of the total cell surface area. Cell contacts dominated by the L3-12 TCR were unaffected by low levels of rCD2 but increased in the presence of higher levels of rCD2 when $B_{rCD2} > 300$ molecules/μm^2 (**Figure 3B**). The measured p-values for rCD2 without L3-12 TCR at the SLB were similar to previously measured contact sizes, ranging from $0.05 < p < 0.1$, for contacts containing rCD2 and various forms of rat CD48 (**Figure 3C**) (Dustin et al., 1997; Jönsson et al., 2016; Zhu et al., 2007). However, the contact size increased considerably in the presence of the L3-12 TCR (**Figure 3C**) and approximately doubled in size at $B_{TCR} > 900$ molecules/μm^2 (**Figure 3C**). The increase in contact area was dependent on the amount of bound ligands, which in this study was dominated by the L3-12 TCR binding to HLA-DQ8-glia-α1 since the Jurkat T cells had approximately four times more HLA-DQ8-glia-α1 than $rCD48_{T92A}$ (**Table 1**).

Increased apparent ligand binding at high ligand densities

Above a contact size of approximately $p = 0.2$ the bound cells formed lamellipodia, with larger lamellipodia forming at higher $B \times p$ values (**Figure 3**). In the Zhu-Golan plots these points were typically shifted to the right with only a minor decrease in B/F with increasing $B \times p$ (**Figure 4**). For rCD2 it was only in combination with L3-12 TCR in the SLB that the Zhu-Golan plot showed this behavior (**Figure 4D**). rCD2 alone did not lead to contact formation larger than 15% of the total cell surface area and no clear lamellipodia, suggesting a possible correlation between lamellipodia formation and the increased apparent binding (**Figure 4C and D**). Another possible contributing factor for the increased binding is that cooperative interactions at the higher ligand densities occur, which leads to an elevated affinity (Steinkühler et al., 2019). However, for the Zhu-Golan points at the highest $B \times p$ values the total amount of bound receptors exceeds the total receptor number, N_{tot} in Table 1, indicating that cooperative binding alone cannot explain the increased binding. If the receptor-ligand affinity is assumed to be unchanged the number of cell surface receptors increases by up to 50% for the highest ligand

densities in Figure 4. To investigate whether the increased apparent binding was caused by trapped ligands under the cells a mobility study was conducted using FRAP (**Figure S3**). Both the L3-12 TCR and the rCD2 in the contact recovered almost completely within 40 seconds with 89±15% and 90±13% recovery for the L3-12 TCR and rCD2, respectively. This indicates that the increased binding under the lamellipodia conditions are not due to trapped ligands under the cells but could instead originate from an increased number of receptors.

To further investigate the role of lamellipodia formation, the cells were treated with latrunculin A, an actin polymerization inhibitor. Since the largest contact areas, and thus most pronounced binding levels were observed on mixtures containing both L3-12 TCR and rCD2 (**Figure 3**), latrunculin A treated cells were added to SLBs containing both proteins. The treated cells changed shape and formed larger cell-SLB contacts without observable lamellipodia (**Figure S4**). Moreover, the contact areas were of similar size with an average *p*-value of 0.24±0.07, independent of the ligand density at the SLB. The maximum number of bound ligands in the contacts decreased for both rCD2 and L3-12 TCR by 40% (**Figure S4**). This was also the case for SLBs functionalized with only one type of ligand (**data not shown**). Furthermore, no increased ligand binding above X, with X defining the point on the Zhu-Golan curve where $B/F = 0$ corresponding to all receptors being bound, was observed for the latrunculin A-treated cells at the concentrations of L3-12 TCR and rCD2 that, for untreated cells, gave rise to this effect (**Figure S4**). This is in agreement with the formation of lamellipodia being a key event in producing increased ligand binding.

Discussion

Measuring 2D K_d values is considerably less common than measuring their 3D counterparts. However, it has become increasingly clear that there is not always a one-to-one relation between 2D and 3D affinities (Huang et al., 2010; Huppa et al., 2010), and in order to be able to accurately model the behavior of immune-cell signaling we need to know the former. Obtaining 2D K_d values has typically been done using either a mechanical approach based on micropipettes to periodically bring cells presenting the two proteins into contact (Huang et al., 2010) or using fluorescence-based methods.

We have chosen to use the fluorescence-based Zhu-Golan method (**Figure 5A**), which allows weak interactions to be measured as well as the effects of auxiliary ligands to be studied. In this method the density of bound receptors in the flat cell-SLB contact, which is given experimentally by the density of bound ligands, is compared to the free receptor density on the cell surface. The latter is independent of the actual cell surface area in the contact (Zhu et al.,

2007), which can be larger than the cell-SLB contact area due to cell surface roughness (Mege et al., 1986). Therefore, only free receptors in the actual cell-SLB contact are counted. In this way we measured the 2D K_d of L3-12 TCR binding to the celiac disease-related HLA-DQ8-glia-α1 as 14±5 molecules/μm^2. It should be pointed out that this value corresponds to the 2D K_d for the TCR-MHC interaction in our controlled system. The influence of, among others, cell signaling, cytoskeletal interactions, co-receptors, and interactions with the CD3 complex are here omitted, and how these would influence the 2D K_d value can only be a matter of speculation. The obtained 2D K_d value is nonetheless of comparable magnitude to previously measured 2D K_d values for TCRs binding agonist MHCs (Grakoui et al., 1999; Huang et al., 2010; Pielak et al., 2017). Notably, the L3-12 TCR binding HLA-DQ8-glia-α1 2D affinity was 2.3-fold lower than that of rCD2 binding the high affinity rCD48$_{T92A}$ mutant, whereas the corresponding 3D affinity was 1.6-fold higher. Thus, it should again be stressed that there is no direct relationship between 2D and 3D affinities. Different theoretical studies (Hu et al., 2013; Weikl et al., 2019) as well as experiments on cell-derived giant vesicles (Steinkühler et al., 2019) have indicated that membrane fluctuations can influence the 2D K_d value such that it varies with molecular concentration. We did not observe this effect here and instead a single 2D K_d value fitted the data points well, up until the formation of lamellipodia. This indicates that topographical effects due to membrane fluctuations do not have a significant influence on the affinity of our system at the molecular concentrations used in this study.

In addition to TCR-MHC interactions, there are also various auxiliary molecules binding across cell contacts *in vivo*. To investigate whether auxiliary molecules can influence the affinity of other binding pairs we studied how different concentrations of rCD2 binding to rCD48$_{T92A}$ affect the Zhu-Golan plot for the L3-12 TCR binding HLA-DQ8-glia-α1 and *vice versa*. It was found that the affinity was unaffected at lower densities, whereas it could be reduced by up to a factor of two at high densities of bound auxiliary molecules (**Figure 5B**). However, there did not seem to be a universal threshold between “low” and “high”, which was more than a factor of two different depending on whether the auxiliary molecule was rCD2 or if it was L3-12 TCR. The concentration at which the auxiliary ligands lower the affinity might be cell dependent, since we, in a previous study (Jönsson et al., 2016), did not observe any significant change in the binding of human CD4 (hCD4) to MHC class II molecules on Raji B cells, when the densities of the auxiliary molecule human CD2, which binds human CD58, was varied between 200 molecules/μm^2 < B_{CD2} < 1200 molecules/μm^2 (data not shown). To investigate this further we replaced the L3-12 TCR with hCD4 at the SLB and studied its binding to the MHC class II molecule HLA-DQ8-glia-α1 on the transfected Jurkat cells in the

presence of low and high rCD2. It was found that by increasing the rCD2 concentration from B_{rCD2} = 120±40 molecules/μm^2 to 540±160 molecules/μm^2 the average *B/F*-value of hCD4 in the cell-SLB contact decreased by a factor of 1.8 (**Figure S5**). This decrease in effective affinity is similar to that observed for L3-12 TCR binding HLA-DQ8-glia-α1. It was also observed that higher rCD2 concentrations caused increased hCD4 exclusion from the cell-SLB contact (from 25% exclusion at low rCD2 densities to 41% exclusion at high rCD2 densities). The increased exclusion will result in a decrease in the effective affinity and is thus one possible explanation for the decrease in binding when having higher densities of rCD2. Another possibility is that the auxiliary molecules create a less favorable environment for the studied ligand-receptor pair, thus influencing the binding on- and/or off-rates for the investigated interaction, thereby lowering the affinity.

It is generally suggested that adhesion molecules such as CD2 aid in forming cell-cell contacts and by doing so promote binding of lower affinity, or less prevalent, molecules in the cell-cell contact, such as CD4 binding MHC class II molecules (Jönsson et al., 2016) or TCR binding to MHC presenting cognate antigens (Davis and van der Merwe, 2006; James and Vale, 2012; Milstein et al., 2008; Shaw and Dustin, 1997). This is also observed here for hCD4 binding HLA-DQ8-glia-α1, which requires rCD2 in the SLB to form contacts, and would have been expected also for L3-12 TCR binding HLA-DQ8-glia-α1 if the density of the latter had been at physiological levels (100-300 cognate MHC molecules per cell instead of 450 000 MHC molecules (Grakoui et al., 1999; Harding and Unanue, 1990)). The observation that high densities of rCD2 decreases the effective affinity suggests that there is an optimal density range within which rCD2 promotes contact formation but without decreasing the affinities of other interactions. Whether this actually happens *in vivo* can at the moment only be considered speculatively, however, it is noteworthy that physiological densities of rCD2 (hCD2) and rCD48 (hCD58) are 50 to 100 molecules/μm^2 (Dustin et al., 2007; Von Bergwelt-Baildon et al., 2002; Zhu et al., 2006; Zhu et al., 2007), which are comparable to the densities of rCD48$_{T92A}$ on the cells (180 molecules/μm^2) and of rCD2 in the SLB (20-100 molecules/μm^2) used in this study. Since the expression level *in vivo* is similar to the threshold between low and high densities found in this study, it is possible that CD2 could potentially both align the T-cell surface with the antigen presenting cell to support the formation of TCR-MHC bonds, as well as, when enough auxiliary molecules have accumulated in the contact, lower the effective affinity of the TCR-MHC interaction. However, if auxiliary binding molecules influence the affinity *in vivo*, then this also raises the question: which is the correct affinity to measure? There are multiple ligand-receptor pairs acting simultaneously in cell-cell contacts between immune

cells *in vivo* (Huppa and Davis, 2013). It is thus possible that the affinity of a specific ligand-receptor pair at physiological densities of auxiliary molecules deviates from the affinity measured for a system containing only the studied ligand-receptor pair. In addition, if the *in vivo* affinity depends on the density of auxiliary molecules it is possible that the cell could modulate the affinity of a specific ligand-receptor interaction by varying the local density of auxiliary binding pairs.

We also found that the cell-SLB contact size increased monotonically with the number of bound ligands. This increase in contact size did not influence the binding behavior of the ligands significantly at *p*-values less than 0.2, however, at high levels of free ligands, the cells started to form lamellipodia which coincided with an apparent increase in the number of bound ligands in the SLB, by as much as 50% for the largest cell contacts. At these high ligand densities the initially linear Zhu-Golan curve started to level off (**Figure 5C**). One possible cause of the apparent increase of receptors on the cell surface is that the rate of receptor recycling is reduced upon lamellipodia formation, given that it is likely an active site of cytoplasmic rearrangement. It has previously been shown that cell activation can lead to a 1.5-fold increase in the number of cell surface receptors, which were argued to be transiently stored in cytoplasmic vesicles (Thatte et al., 1994; Zhu et al., 2006). Additional cell-membrane receptors that are stored within these cytoplasmic vesicles could also be the source of the "extra" receptors on the cell surface. Prominent, but T-cell activation independent, vesicular fusion linked to the formation of the lamellipodia might have an important role since experiments with the actin-polymerizing drug latrunculin A abolished both lamellipodia formation as well as the high-density binding. The increased amount of bound ligands was, however, not due to trapped ligands since FRAP measurements showed that the majority of ligands in the cell contact were mobile with an effective diffusion coefficient of $D = 0.3 \pm 0.05$ $\mu m^2\ s^{-1}$ and $D = 0.6 \pm 0.13$ $\mu m^2\ s^{-1}$ for L3-12 TCR and rCD2, respectively. These FRAP measurements also set an upper limit to the lifetime of the L3-12 TCR binding HLA-DQ8-glia-α1 and rCD2 binding $rCD48_{T92A}$ interactions, corresponding to 9.5±3 seconds and 7±2 seconds, respectively. These are in the range of intermediate lifetimes (Axmann et al., 2012; Huppa et al., 2010; Lin et al., 2019), indicating that it is mainly a large on-rate that elevates the affinity of L3-12 TCR binding to HLA-DQ8-glia-α1. It should finally be noted that we do not see a significant influence of topographical effects in the binding studies, which would be expected to show up as a non-linear distortion of the Zhu-Golan plot. However, it is possible that a reduction of membrane fluctuations at high ligand densities contributes to the increased binding we observe for these data points.

In summary, our study shows that 2D affinities do not only depend on the protein-protein interaction per se but also on several other factors such as auxiliary binding molecules, ligand density and the dynamic behavior of the cell. Although measurements of ligand to receptor binding for soluble molecules have provided vital information about how our immune system distinguishes between self, transformed self (for example neo-epitopes) and non-self, it is clear that a better understanding of how different factors affect binding in cell contacts will help with modelling these processes with even higher accuracy. The results obtained here take a step in this direction, helping to understand the effect of cellular context, and in particular auxiliary binding molecules, on the affinities of ligand-receptor interactions at cell-cell contacts.

Materials and Methods

Cell lines and culture

The human E6.1 Jurkat T-cell line was cultured in 1640 RPMI media (#R8758, Sigma) supplemented with 10% fetal bovine serum (FBS, #F9665, Sigma), 2.05 mM L-Glutamine (#G7513, Sigma), 1 mM Sodium Pyruvate (#S8636, Sigma), 1% HEPES (#H0887, Sigma), 1% of Penicillin (c_{stock} = 5000 units mL^{-1}) and Streptomycin (c_{stock} = 5000 µg mL^{-1}) (#P4083, Sigma) at 5% CO_2 and 37°C. These cells were transduced using a lentivirus to express the rCD48 mutant T92A and the human MHC class II molecule HLA-DQ8 (DQA1*0301; DQB1*0302) attached covalently to the α1-gliadin peptide (PSGEGSFQPSQENPQ) and cultured as above. The cells were kept at a cell density between 0.5×10^6 - 0.8×10^6 cells mL^{-1} between each experiment. Human embryonic kidney 293T (HEK293T) cells were cultured in DMEM media (#41966029, Thermo Fisher Scientific) supplemented with 10% FBS, 2.05 mM L-Glutamine, 1% HEPES, 1% of Penicillin (c_{stock} = 5000 units mL^{-1}) and Streptomycin (c_{stock} = 5000 µg mL^{-1}) at 5% CO_2 and 37°C. HEK293T cells were used for lentivirus production only. All cells were subcultured every 2-3 days.

Stably-transduced Jurkat T cells

4×10^5 cells mL^{-1} HEK293T cells were plated in a 6-well plate and incubated overnight at 5% CO_2 and 37°C in supplemented DMEM media. After 24 hours the HEK293T cells reached a confluency of 80% and were transfected with 0.5 µg of the pHR-SIN lentiviral expression vector containing the DNA of interest (HLA-DQ8-glia-α1 or $rCD48_{T92A}$) mixed with 0.5 µg of each of the packaging vectors p8.91 and pMD.G (2^{nd} Generation) using GeneJuice® (#70967,

MERCK) according to the manufacturer's instructions. The supernatant containing virus particles was harvested 72 hours post transfection at 5% CO_2 and 37°C and centrifuged for 15 minutes at 3000 rpm (Eppendorf Centrifuge 5810R, #EP022628188, Sigma) to separate cell debris from the lentiviral-conditioned medium. 1.5 mL of the lentiviral-conditioned medium were subsequently added to 1×10^6 Jurkat T cells and the expression of the transfected proteins tested three days after using flow cytometry.

Flow cytometry

0.5×10^6 cells were centrifuged at 4°C for two minutes, 1200 rpm (Heraeus™ Multifuge™ X1R, Thermo Fisher Scientific) and washed twice with HEPES Buffer Saline (HBS) buffer (150 mM NaCl (#7647-14-5, VWR), 10 mM 2-[4-(2-hydroxyethyl)piperazin-1-yl]ethanesulfonic acid (HEPES, #H3375, Sigma), pH 7.4) containing 0.05% sodium azide. The cells were labelled with either the isotype phycoerythrin (PE) anti-mouse IgG1 (clone MOPC-21, #400112, BioLegend®, 1:5 and 1:10 dilution), PE-anti-human HLA-DQ (clone HLADQ1, #318106 BioLegend®, 1:5 dilution) or PE-anti-rat CD48 (clone OX-45, #MA5-17528, Thermo Fisher Scientific, 1:10 dilution) for 45 minutes on ice and afterwards washed twice with HBS buffer + 0.05% sodium azide. An initial antibody titration experiment was conducted to assess the antibody concentrations for optimal antigen binding. For quantification purpose BD Quantibrite™ PE beads (#340495, BD Biosciences) were diluted in 300 µL HBS buffer + 0.05% sodium azide and measured alongside with the antibody-stained cells in a BD Accuri™ C6 Flow Cytometer (BD Biosciences). This allowed for the calculation of the total number of antibodies per cell, which, at saturating concentrations of antibodies, was assumed to be equal to the total number of receptors per cell (Poncelet and Carayon, 1985). All data were analyzed using FlowJo™ (v10.5.2, BD Biosciences) and Microsoft Excel (Microsoft).

Vesicle preparation

Vesicle solutions containing 5 wt% (10 wt% for the hCD4 experiments) 1,2-dioleoyl-sn-glycero-3-[(N-(5-amino-1-carboxypentyl)iminodiacetic acid)succinyl] (nickel salt) (DGS-NTA, #790404C, Avanti® Polar Lipids, Inc) and 95 wt% (90 wt% for the hCD4 measurements) 1-palmitoyl-2-oleoyl-glycero-3-phosphocholine (POPC, #850457C, Avanti® Polar Lipids, Inc, USA) were prepared at a total lipid concentration of 0.5 mg mL^{-1}. First, the different lipids were mixed in 100 µL chloroform and then dried to remove the chloroform by using a N_2 gas flow for 10 minutes. The dried lipids were re-suspended and thoroughly mixed in 1 mL of filtered (0.2 µm Minisart® Syringe filter, Sartorius, #16534K, Sigma) HBS buffer and incubated on ice

for 1-2 hours. To create small unilamellar vesicles, the vesicle solution was tip sonicated with a CV18 model tip sonicator (Chemical instruments AB) for 15 minutes with a pulse time of 10 seconds and an amplitude of 55%. The vesicle solutions were stored at 4°C until used and renewed every month.

Supported lipid bilayers

For the formation of SLBs 0.15 mm thick, round glass slides (number one coverslips, Ø 25 mm, #CB00150RA020MNT0, Thermo Fisher Scientific) were used as support. All glass slides were cleaned for 30 minutes in 80°C heated piranha solution (mixture of 75% sulfuric acid (99.9%, #100731, Merck) and 25% hydrogen peroxide (30%, #H1009, Sigma)). After the piranha cleaning the glass slides were rinsed for one minute with deionized water and dried using N_2 gas. Silicon wells (Silicon isolators, 12 × 4.5 mm diameter, 1.7 mm depth; SKU: 665206, Grace Biolabs, USA) were attached to the glass slide by pressing the clean glass onto the silicon well. Next, 30 µL HBS buffer was added to the wells followed by 30 µL of a 1:10 dilution of the vesicles in HBS buffer. After the addition to the prepared well the vesicles were incubated for one hour at room temperature (RT) to allow for the formation of a fluid and continuous SLB on the glass surface. The SLB was washed five times with 50 µL HBS buffer to rinse away non-ruptured vesicles. The ability of the lipids to form SLBs was confirmed using FRAP as previously described (Junghans et al., 2018).

Affinity measurements

A histidine tag covalently bound to the proteins allowed for binding of rCD2 and L3-12 TCR to DGS-NTA lipids in the SLB. Recombinant rCD2 and hCD4 were produced as in reference (Chang et al., 2016; Jönsson et al., 2016) and were genetically modified at the C-terminus with a double histidine tag (12xH) or with a single histidine tag (6xH), respectively, while the human L3-12 TCR had one histidine tag (6xH) each on the C-terminus of the α and β chain. The L3-12 TCR was produced as described by Broughton *et al.* (Broughton et al., 2012). All proteins were fluorescently labelled using an Alexa Fluor® antibody labelling kit from Thermo Fisher Scientific (#A20181 and #A10475) with a labelling efficiency in the range 1.1 to 1.7 Alexa Fluor® molecules per protein. The L3-12 TCR and hCD4 were labelled with Alexa Fluor® 488 and the rCD2 with Alexa Fluor® 647. For the L3-12 TCR and rCD2 experiments both proteins were diluted in HBS buffer and added either i) as single proteins or ii) in combination to the SLB. Both the formation of SLBs and the subsequent binding of proteins was prepared at RT. After 45 minutes of incubation the proteins were washed off and the sample moved to a 37°C

temperature chamber. To allow for the sample to heat up to 37°C it was incubated for 5-7 minutes before the addition of 37°C warm Jurkat T cells expressing HLA-DQ8-glia-α1 and $rCD48_{T92A}$. The Jurkat T cells were incubated on the SLB in supplemented RPMI containing 10% FBS to reduce unspecific cell-SLB adhesion (Movie S5). The ligands in the SLB were still mobile after the addition of supplemented RPMI as confirmed by FRAP. Contact growth and protein binding reached steady state after 15 minutes incubation and the SLB was washed five times with 50 µL HBS buffer to rinse away unbound cells and traces of cell media. Increasing amounts of the labelled L3-12 TCR and/or rCD2 were added to the SLB and were incubated for 20 minutes after the cells had bound. Images were captured after washing off unbound proteins. This was repeated three to four times for each SLB. All images were acquired on a Zeiss observer Z1 TIRF microscope (Plan-Apochromat 100x, NA = 1.46 objective, Zeiss, Germany) equipped with a Hamamatsu ORCA-Flash4.0 LT Digital CMOS camera (C11440-42U) and Slidebook 5.5 as the operating software. A 3i solid state diode laser stack operating at a wavelength of 488 nm (100 mW) and 638 nm (100 mW) (3il33, Denver, Colorado USA) were used to illuminate the sample together with a 446/523/600/677 nm TIRF quad-band dichroic filter cube. All these measurements were carried out at 37°C. The hCD4 measurements were done at RT and the bound cells were incubated for 40 minutes before the images were acquired with a Nikon Eclipse Ti microscope using a 100x magnification oil immersion objective (Plan Apo TIRF, N.A. 1.45, Nikon Corporation, Japan), a back-illuminated scientific CMOS camera (Prime 95B, Photometrics, USA), 488 nm and 638 nm diode lasers (LBX, Oxxius, France) with a 531/46 nm BrightLine® single-band bandpass filter and a 635 nm laser BrightLine® single-edge laser dichroic beamsplitter (Semrock, USA), respectively.

Latrunculin A treatment

1×10^6 transfected Jurkat T cells were incubated in 1 mL supplemented RPMI 1640 media containing 25 µM Latrunculin A (# ab144290, Abcam, Sweden) for two hours at 37°C. The cells were then added as described above to the SLB. All subsequent washing steps on the SLB were done in HBS buffer containing 25 µM Latrunculin A to allow for an effective drug response throughout the complete measurement.

Fluorescence recovery measurements

FRAP measurements were done for both (i) receptors on stained, transfected Jurkat T cells and (ii) fluorescently-labelled recombinant proteins in a cell-SLB contact. (i) PE α-human HLA-DQ or PE α-rat CD48 labelled Jurkat T cells (labelling protocol see *Flow Cytometry*) were used

to gain the mobile fraction f of the receptors on the T-cell surface, and (ii) functionalized SLBs with L3-12 TCR or rCD2 binding to their corresponding receptors on Jurkat T cells were used to gain the mobile fraction of the ligands within the contact area, $f_{contact}$, as well as to estimate the diffusion coefficient of ligands in the contact and the lifetime of the ligand-receptor interaction. Images were acquired with an CSU-X1 spinning disc confocal microscope (Plan-Apochromat 100x, NA = 1.46 objective, Zeiss, Germany), an Evolve EMCCD (512×512) camera, a 3i solid state diode laser stack operating at a wavelength of 488 nm (100 mW) and 638 nm (100 mW) (3il33, Denver, Colorado USA) with a GFP confocal emission filter (524/30) and an RFP confocal emission filter (617/73). A series of pre-bleached images was taken before a full laser power bleach of <50 ms was conducted. The recovery was followed for (i) 250 seconds or (ii) 120 seconds. To calculate the mobile fraction the intensity of an area in the bleached spot, I_{bleach}, as well as outside the bleached spot along the membrane or within the contact area, $I_{control}$, was measured over the course of recovery. To account for fluorophore bleaching during recovery, I_{bleach} was normalized by $I_{control}$. The normalized total intensity over time $I_{tot}(t)$ reached steady state after 40-50 seconds and the normalized intensity ratio at steady state gave the mobile fraction. The diffusion coefficient, D, was calculated from the recovery curve by fitting the intensities over time according to Eqn. 20 in Jönsson *et al.* (Jönsson et al., 2008).

Conversion of intensities to molecules/µm^2

The single-molecule values were measured as previously described (Junghans et al., 2018). Briefly, a 1 pM solution of labelled proteins was added to a glass cover slide resulting in approximately 100 protein molecules binding randomly in the microscope field of view. Single molecules were detected and counted and the sum of the intensity from each molecule was determined and subtracted with the average intensity outside the molecules to correct for non-zero background. This was done at several different days and if no single molecule value was taken on a specific experimental day an average of single molecule values around that day were used. To convert the fluorescence intensity per pixel, I, to protein density, c, the following expression was used:

$$c = \frac{I}{A_{\mathrm{spot}} \times I_{\mathrm{spot}}} \qquad \textbf{(2)}$$

where I_{spot} is the average intensity from the single molecule within the area A_{spot} under the same illumination and microscope settings as used in the cell-SLB experiments.

Zhu-Golan analysis

The 2D K_d of the ligand-receptor interactions was obtained from the negative reciprocal of the slope of a B/F vs $B \times p$ plot, a so-called Zhu-Golan plot. The intercept of the Zhu-Golan plot with the x-axis also gave the total number of receptors on the cell surface, N_{tot}, from:

$$N_{tot} = \frac{X \times S_{cell}}{f} \quad \textbf{(3)}$$

where X is the point on the Zhu-Golan curve where $B/F = 0$. S_{cell} was calculated according to:

$$S_{cell} = 4\pi r^2 \times 1.8 \quad \textbf{(4)}$$

where r is the average radius of the cell obtained from widefield images and the factor 1.8 accounts for cell surface roughness (Mege et al., 1986). S_{cell} was on average 700±100 μm^2. Whereas $N_{tot} \times f$ was free to vary for the single ligand analysis it was fixed to the value determined for the single ligands when fitting data including the auxiliary ligands. To estimate the increase in the amounts of bound ligands observed in large contact areas, the calculated K_d curves from the Zhu-Golan plot for the single ligands were shifted to the right until they passed through the investigated data point in the Zhu-Golan plot. This resulted in new x-intercepts and hence N_{tot} values that were used to calculate the number of bound ligands. The cell-SLB contact area, S_b, was defined by areas of increased ligand intensity on the SLB. The outlines of the cell contacts were created by subtracting the background from the images using a rolling ball algorithm and thresholding for high intensity areas. These outlines were then corrected manually for non-binding areas within the cell contact. Once all outlines were obtained, the area and the mean grey intensity values of the fluorescently-labelled ligands in the cell contacts were extracted from raw images of 200-400 cells per experiment (with 50-100 cells per separate concentration). The mean grey values in the contact were corrected for the dark count value and converted into total ligand density in the contact ($B + F$) using the intensity obtained from single-molecule measurements as described above (see *Conversion of intensities to molecules/μm^2*). The free ligand density on the SLB, F*, was obtained from the intensity outside the cell contacts, corrected for the dark count value as well as converted to protein densities. It has previously been found that the free ligand density in the contact area, F, is 10% to 40% lower than the density on the surrounding SLB (Bromley et al., 2001; Dustin et al., 2007; Jönsson et al., 2016; Zhu et al., 2007). This was also observed here when measuring the exclusion of non-binding 1G4 TCR, which decreased by on average 25%, when the contact was formed either with rCD2 binding rCD48$_{T92A}$ or with L3-12 TCR binding HLA-DQ8-glia-α1 (B_{rCD2} = 390 molecules/μm^2 and B_{TCR} = 500 to 1800 molecules/μm^2, with individual contacts ranging from p = 0.01 to p = 0.4). There was no significant difference in the level of exclusion

when having rCD2 compared to L3-12 TCR, nor was there a significant dependence on the exclusion level with contact size, p, for a cell. It was therefore assumed that $F = 0.75F^*$ for all ligands and concentrations, and the number of bound molecules, B, was obtained by:

$$B = B^* - F \quad \textbf{(5)}$$

Potential errors introduced by this approximation have been addressed elsewhere (Jönsson et al., 2016; Zhu et al., 2007). All images were analyzed using Image J (Version 1.49V) and the data were plotted in Prism 8 (GraphPad). If not otherwise indicated all data are presented as the mean value ± the standard deviation (s.d.).

Competing interest

No competing interest declared.

Funding

PJ has received funding from the European Research Council (ERC) under the European Union's Horizon 2020 research and innovation program (Grant agreement No. 757797). SJD is funded by the Wellcome Trust (grant number 098274/Z/12/Z). JR is supported by an Australian Research Council Laureate Fellowship.

Data availability

All raw data in the manuscript are available upon request from the corresponding authors.

References

Alam, S. M., Davies, G. M., Lin, C. M., Zal, T., Nasholds, W., Jameson, S. C., Hogquist, K. A., Gascoigne, N. R. J. and Travers, P. J. (1999). Qualitative and Quantitative Differences in T Cell Receptor Binding of Agonist and Antagonist Ligands. *Immunity* **10**, 227–237.

Axmann, M., Huppa, J. B., Davis, M. M. and Schütz, G. J. (2012). Determination of Interaction Kinetics between the T Cell Receptor and Peptide-Loaded MHC Class II via Single-Molecule Diffusion Measurements. *Biophys. J.* **103**, L17–L19.

Bromley, S. K., Iaboni, A., Davis, S. J., Whitty, A., Green, J. M., Shaw, A. S., Weiss, A. and Dustin, M. L. (2001). The immunological synapse and CD28-CD80 interactions. *Nat. Immunol.* **2**, 1159–1166.

Broughton, S. E., Petersen, J., Theodossis, A., Scally, S. W., Loh, K. L., Thompson, A., van Bergen, J., Kooy-Winkelaar, Y., Henderson, K. N., Beddoe, T., et al. (2012). Biased T Cell Receptor Usage Directed against Human Leukocyte Antigen DQ8-Restricted Gliadin Peptides Is Associated with Celiac Disease. *Immunity* **37**, 611–621.

Bulek, A. M., Cole, D. K., Skowera, A., Dolton, G., Gras, S., Madura, F., Fuller, A., Miles, J. J., Gostick, E., Price, D. A., et al. (2012). Structural basis for the killing of human beta cells by CD8+ T cells in type 1 diabetes. *Nat. Immunol.* **13**, 283–289.

Chakraborty, A. K. and Weiss, A. (2014). Insights into the initiation of TCR signaling. *Nat. Immunol.* **15**, 798–807.

Chang, V. T., Fernandes, R. A., Ganzinger, K. A., Lee, S. F., Siebold, C., McColl, J., Jönsson, P., Palayret, M., Harlos, K., Coles, C. H., et al. (2016). Initiation of T cell signaling by CD45 segregation at 'close contacts'. *Nat. Immunol.* **17**, 574–582.

Choudhuri, K., Llodrá, J., Roth, E. W., Tsai, J., Gordo, S., Wucherpfennig, K. W., Kam, L. C., Stokes, D. L. and Dustin, M. L. (2014). Polarized release of T-cell-receptor-enriched microvesicles at the immunological synapse. *Nature* **507**, 118–123.

Cole, D. K., Pumphrey, N. J., Boulter, J. M., Sami, M., Bell, J. I., Gostick, E., Price, D. A., Gao, G. F., Sewell, A. K. and Jakobsen, B. K. (2007). Human TCR-Binding Affinity is Governed by MHC Class Restriction. *J. Immunol.* **178**, 5727–5734.

Davis, S. J. and van der Merwe, P. A. (2006). The kinetic-segregation model: TCR triggering and beyond. *Nat. Immunol.* **7**, 803–809.

Deng, L. and Mariuzza, R. A. (2007). Recognition of self-peptide-MHC complexes by autoimmune T-cell receptors. *Trends Biochem. Sci.* **32**, 500–508.

Dustin, M. L., Golan, D. E., Zhu, D.-M., Miller, J. M., Meier, W., Davies, E. A. and van der Merwe, P. A. (1997). Low Affinity Interaction of Human or Rat T Cell Adhesion Molecule CD2 with Its Ligand Aligns Adhering Membranes to Achieve High Physiological Affinity. *J. Biol. Chem.* **272**, 30889–30898.

Dustin, M. L., Bromley, S. K., Davis, M. M. and Zhu, C. (2001). Identification of Self Through Two-Dimensional Chemistry and Synapses. *Annu. Rev. Cell Dev. Biol.* **17**, 133–157.

Dustin, M. L., Starr, T., Coombs, D., Majeau, G. R., Meier, W., Hochman, P. S., Douglass, A., Vale, R., Goldstein, B. and Whitty, A. (2007). Quantification and modeling of tripartite CD2-, CD58FC chimera (Alefacept)-, and CD16-mediated cell adhesion. *J. Biol. Chem.* **282**, 34748–34757.

Evans, E. J., Castro, M. A. A., O'Brien, R., Kearney, A., Walsh, H., Sparks, L. M., Tucknott, M. G., Davies, E. A., Carmo, A. M., van der Merwe, P. A., et al. (2006). Crystal Structure and Binding Properties of the CD2 and CD244 (2B4)-binding Protein, CD48. *J. Biol. Chem.* **281**, 29309–29320.

Garcia, K. C., Tallquist, M. D., Pease, L. R., Brunmark, A., Scott, C. A., Degano, M., Stura, E. A., Peterson, P. A., Wilson, I. A. and Teyton, L. (1997). T cell receptor interactions with syngeneic and allogeneic ligands: Affinity measurements and crystallization. *Proc. Natl. Acad. Sci.* **94**, 13838–13843.

Grakoui, A., Bromley, S. K., Sumen, C., Davis, M. M., Shaw, A. S., Allen, P. M. and Dustin, M. L. (1999). The immunological synapse: A molecular machine controlling T cell activation. *Science* **285**, 221–227.

Harding, C. V. and Unanue, E. R. (1990). Quantitation of antigen-presenting cell MHC class II/peptide complexes necessary for T-cell stimulation. *Nature* **346**, 574–576.

Hu, J., Lipowsky, R. and Weikl, T. R. (2013). Binding constants of membrane-anchored receptors and ligands depend strongly on the nanoscale roughness of membranes. *Proc. Natl. Acad. Sci.* **110**, 15283–15288.

Huang, J., Zarnitsyna, V. I., Liu, B., Edwards, L. J., Jiang, N., Evavold, B. D. and Zhu, C. (2010). The kinetics of two-dimensional TCR and pMHC interactions determine T-cell responsiveness. *Nature* **464**, 932–936.

Huppa, J. B. and Davis, M. M. (2013). The Interdisciplinary Science of T-cell Recognition. In *Advances in Immunology*, pp. 1–50.

Huppa, J. B., Axmann, M., Mörtelmaier, M. A., Lillemeier, B. F., Newell, E. W., Brameshuber, M., Klein, L. O., Schütz, G. J. and Davis, M. M. (2010). TCR–peptide–MHC interactions in situ show accelerated kinetics and increased affinity. *Nature* **463**, 963–967.

James, J. R. and Vale, R. D. (2012). Biophysical mechanism of T-cell receptor triggering in a reconstituted system. *Nature* **487**, 64–69.

Jönsson, P., Jonsson, M. P., Tegenfeldt, J. O. and Höök, F. (2008). A Method Improving the Accuracy of Fluorescence Recovery after Photobleaching Analysis. *Biophys. J.* **95**, 5334–5348.

Jönsson, P., Southcombe, J. H., Santos, A. M., Huo, J., Fernandes, R. A., McColl, J., Lever, M., Evans, E. J., Hudson, A., Chang, V. T., et al. (2016). Remarkably low affinity of CD4/peptide-major histocompatibility complex class II protein interactions. *Proc. Natl. Acad. Sci.* **113**, 5682–5687.

Junghans, V., Hladilkova, J., Santos, A. M., Lund, M., Davis, S. J. and Jönsson, P. (2018). Hydrodynamic trapping measures the interaction between membrane-associated molecules. *Sci. Rep.* **8**, 12479.

Limozin, L., Bridge, M., Bongrand, P., Dushek, O., van der Merwe, P. A. and Robert, P. (2019). TCR–pMHC kinetics under force in a cell-free system show no intrinsic catch bond, but a minimal encounter duration before binding. *Proc. Natl. Acad. Sci.* **116**, 16943–16948.

Lin, J. J. Y., Low-Nam, S. T., Alfieri, K. N., McAffee, D. B., Fay, N. C. and Groves, J. T. (2019). Mapping the stochastic sequence of individual ligand-receptor binding events to cellular activation: T cells act on the rare events. *Sci. Signal.* **12**, eaat8715.

Matsui, K., Boniface, J. J., Steffner, P., Reay, P. A. and Davis, M. M. (1994). Kinetics of T-cell receptor binding to peptide/I-Ek complexes: correlation of the dissociation rate with T-cell responsiveness. *Proc. Natl. Acad. Sci.* **91**, 12862–12866.

Mege, J. L., Capo, C., Benoliel, A. M., Foa, C., Galindo, R. and Bongrand, P. (1986). Quantification of cell surface roughness; a method for studying cell mechanical and adhesive properties. *J. Theor. Biol.* **119**, 147–160.

Milstein, O., Tseng, S.-Y., Starr, T., Llodra, J., Nans, A., Liu, M., Wild, M. K., van der Merwe, P. A., Stokes, D. L., Reisner, Y., et al. (2008). Nanoscale Increases in CD2-CD48-mediated Intermembrane Spacing Decrease Adhesion and Reorganize the Immunological Synapse. *J. Biol. Chem.* **283**, 34414–34422.

Morris, G. P. and Allen, P. M. (2012). How the TCR balances sensitivity and specificity for the recognition of self and pathogens. *Nat. Immunol.* **13**, 121–128.

Negulescu, P. A., Krasieva, T. B., Khan, A., Kerschbaum, H. H. and Cahalan, M. D. (1996). Polarity of T Cell Shape, Motility, and Sensitivity to Antigen. *Immunity* **4**, 421–430.

O'Donoghue, G. P., Pielak, R. M., Smoligovets, A. A., Lin, J. J. and Groves, J. T. (2013). Direct single molecule measurement of TCR triggering by agonist pMHC in living primary T cells. *Elife* **2**, e00778.

Pielak, R. M., O'Donoghue, G. P., Lin, J. J., Alfieri, K. N., Fay, N. C., Low-Nam, S. T. and Groves, J. T. (2017). Early T cell receptor signals globally modulate ligand:receptor affinities during antigen discrimination. *Proc. Natl. Acad. Sci.* **114**, 12190–12195.

Poncelet, P. and Carayon, P. (1985). Cytofluorometric quantification of cell-surface antigens by indirect immunofluorescence using monoclonal antibodies. *J. Immunol. Methods* **85**, 65–74.

Rosette, C., Werlen, G., Daniels, M. A., Holman, P. O., Alam, S. M., Travers, P. J., Gascoigne, N. R. J., Palmer, E. and Jameson, S. C. (2001). The Impact of Duration versus Extent of TCR Occupancy on T Cell Activation. *Immunity* **15**, 59–70.

Rossjohn, J., Gras, S., Miles, J. J., Turner, S. J., Godfrey, D. I. and McCluskey, J. (2015). T Cell Antigen Receptor Recognition of Antigen-Presenting Molecules. *Annu. Rev. Immunol.* **33**, 169–200.

Shao, J.-Y., Yu, Y. and Dustin, M. L. (2005). A Model for CD2/CD58-Mediated Adhesion Strengthening. *Ann. Biomed. Eng.* **33**, 483–493.

Shaw, A. S. and Dustin, M. L. (1997). Making the T cell receptor go the distance: A topological view of T cell activation. *Immunity* **6**, 361–369.

Steinkühler, J., Rózycki, B., Alvey, C., Lipowsky, R., Weikl, T. R., Dimova, R. and Discher, D. E. (2019). Membrane fluctuations and acidosis regulate cooperative binding of 'marker of self' protein CD47 with the macrophage checkpoint receptor SIRPα. *J. Cell Sci.* **132**, jcs216770.

Stone, J. D., Chervin, A. S. and Kranz, D. M. (2009). T-cell receptor binding affinities and kinetics: impact on T-cell activity and specificity. *Immunology* **126**, 165–176.

Sumen, C., Dustin, M. L. and Davis, M. M. (2004). T cell receptor antagonism interferes with MHC clustering and integrin patterning during immunological synapse formation. *J. Cell Biol.* **166**, 579–590.

Thatte, H. S., Bridges, K. R. and Golan, D. E. (1994). Microtubule inhibitors differentially affect translational movement, cell surface expression, and endocytosis of transferrin receptors in K562 cells. *J. Cell. Physiol.* **160**, 345–357.

Tolentino, T. P., Wu, J., Zarnitsyna, V. I., Fang, Y., Dustin, M. L. and Zhu, C. (2008). Measuring Diffusion and Binding Kinetics by Contact Area FRAP. *Biophys. J.* **95**, 920–930.

van der Merwe, P. A. and Dushek, O. (2011). Mechanisms for T cell receptor triggering. *Nat. Rev. Immunol.* **11**, 47–55.

Von Bergwelt-Baildon, M. S., Vonderheide, R. H., Maecker, B., Hirano, N., Anderson, K. S., Butler, M. O., Xia, Z., Zeng, W. Y., Wucherpfennig, K. W., Nadler, L. M., et al. (2002). Human primary and memory cytotoxic T lymphocyte responses are efficiently induced by means of CD40-activated B cells as antigen-presenting cells: Potential for clinical application. *Blood* **99**, 3319–3325.

Weikl, T. R., Hu, J., Kav, B. and Różycki, B. (2019). Binding and segregation of proteins in membrane adhesion: theory, modeling, and simulations. In *Advances in Biomembranes and Lipid Self-Assembly*, pp. 159–194.

Xu, G. K., Hu, J., Lipowsky, R. and Weikl, T. R. (2015). Binding constants of membrane-anchored receptors and ligands: A general theory corroborated by Monte Carlo simulations. *J. Chem. Phys.* **143**, 243136.

Zhu, D.-M., Dustin, M. L., Cairo, C. W., Thatte, H. S. and Golan, D. E. (2006). Mechanisms of Cellular Avidity Regulation in CD2–CD58-Mediated T Cell Adhesion. *ACS Chem. Biol.* **1**, 649–658.

Zhu, D.-M., Dustin, M. L., Cairo, C. W. and Golan, D. E. (2007). Analysis of Two-Dimensional Dissociation Constant of Laterally Mobile Cell Adhesion Molecules. *Biophys. J.* **92**, 1022–1034.

Zhu, C., Jiang, N., Huang, J., Zarnitsyna, V. I. and Evavold, B. D. (2013). Insights from in situ analysis of TCR-pMHC recognition: response of an interaction network. *Immunol. Rev.* **251**, 49–64.

Figures

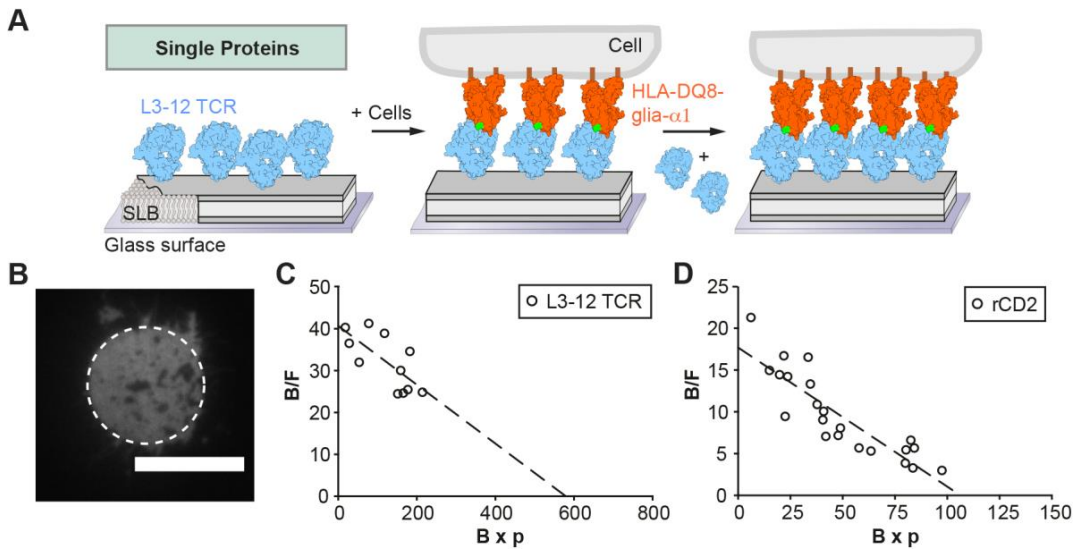

Figure 1. 2D K_d measurements of L3-12 TCR binding HLA-DQ8-glia-α1 and rCD2 binding $rCD48_{T92A}$

(A) Schematic representation of a cell-SLB binding experiment to obtain Zhu-Golan plots of the ligand-receptor interaction. **(B)** Accumulated L3-12 TCR beneath a Jurkat T cell. Cell contour represented by a dashed circle. Scale bar 10 μm. **(C)** Zhu-Golan plot for the L3-12 TCR binding HLA-DQ8-glia-α1, with a 2D K_d of 14±5 molecules/μm^2. Only data points below $B{\times}p$ = 300 molecules/μm^2 are included. **(D)** Zhu-Golan plot for the rCD2 binding $rCD48_{T92A}$ interaction, with a 2D K_d of 6±1 molecules/μm^2. The dashed lines are fits to Eqn. 1. The data points represent an average value for 50-100 analyzed cells and are from six (for L3-12 TCR) and nine (for rCD2) independent experiments.

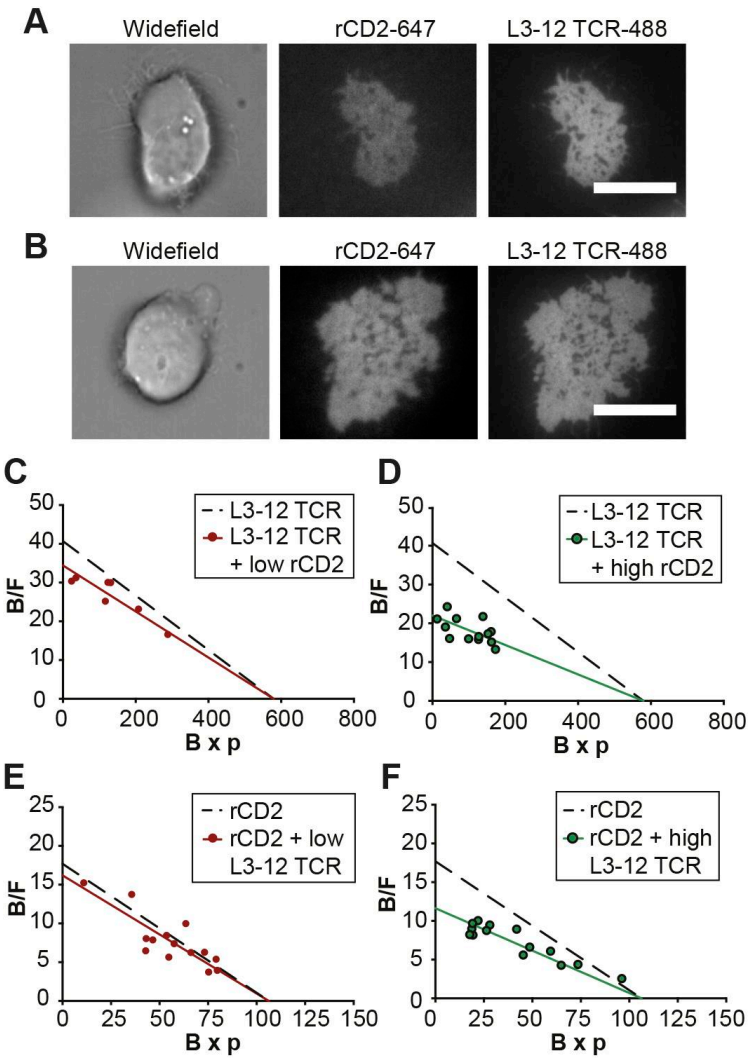

Figure 2. Zhu-Golan analysis for mixtures of L3-12 TCR and rCD2

(A, B) Widefield image of a cell bound to accumulated rCD2 and accumulated L3-12 TCR beneath the cell at (A) low, B_{rCD2} < 200 molecules/μm^2, or (B) high, B_{rCD2} > 300 molecules/μm^2, densities of rCD2. Scale bar is 10 μm. **(C-D)** Zhu-Golan plots for the L3-12 TCR binding HLA-DQ8-glia-α1 at (C) low amounts of CD2 and (D) high amounts of CD2. The dashed line is a fit to the Zhu-Golan plot for the L3-12 TCR only and the solid line to the mixture with rCD2. Only data points below $B{\times}p$ = 300 molecules/μm^2 are included in these figures. **(E-F)** Zhu-Golan plots for rCD2 at (E) low, B_{TCR} < 700 molecules/μm^2, and (F) high, B_{TCR} > 900 molecules/μm^2, densities of L3-12 TCR. The dashed line is a fit to the Zhu-Golan plot for rCD2 only on the SLB and the solid line to the mixture with L3-12 TCR. Only data points below $B{\times}p$ = 100 molecules/μm^2 are included in these figures. Each point represents an average value for 50-100 analyzed cells per *F*-value. Data are from five (C), seven (D and F) and nine (E) independent experiments.

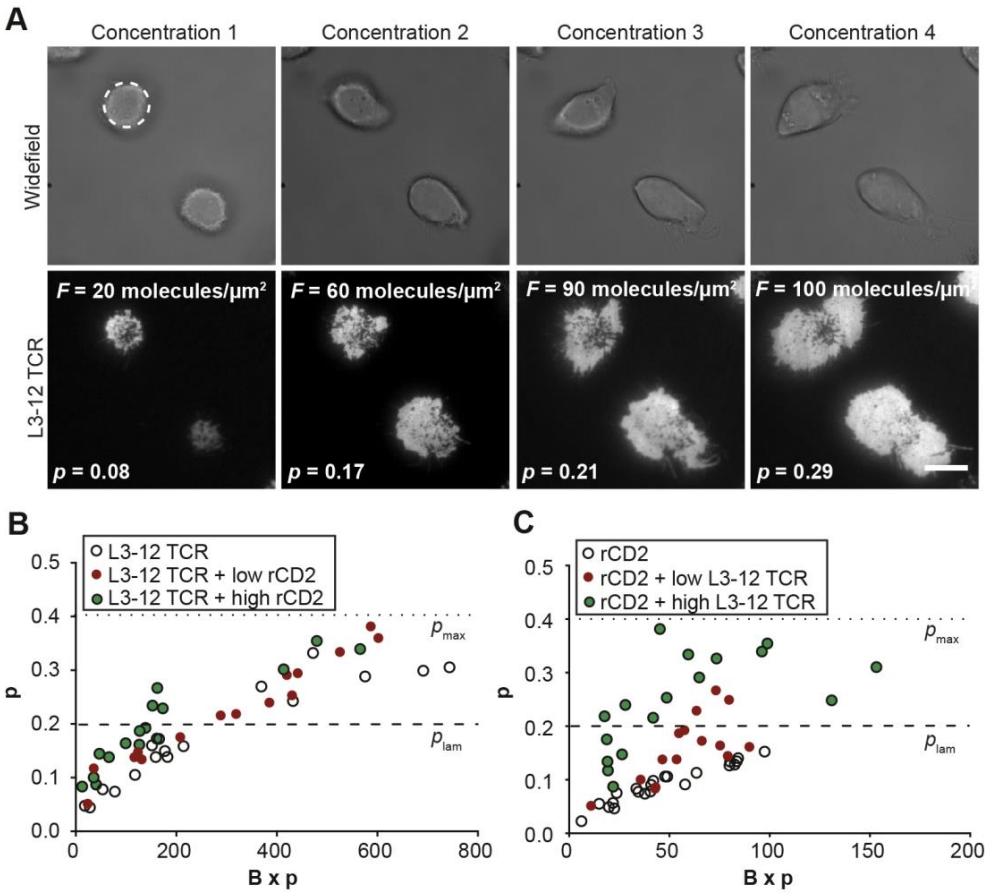

Figure 3. The cell-SLB contact size increases with ligand binding

(A) *Top panel:* Widefield images of two spreading cells on the SLB with increasing concentrations of L3-12 TCR. *Bottom panel*: Accumulated L3-12 TCR beneath the two cells at increasing ligand densities. Scale bar is 10 μm. **(B, C)** Ratio of the contact size to the total cell surface area, *p*, as a function of *B*×*p* for **(B)** the L3-12 TCR in the absence of rCD2 (*empty circles*), the presence of low amounts of rCD2, B_{rCD2} < 200 molecules/μm^2, (*red circles*) or the presence of high amounts of rCD2, B_{rCD2} > 300 molecules/μm^2, (*green circles*). **(C)** rCD2 in the absence of the L3-12 TCR (*empty circles*), the presence of low amounts of L3-12 TCR, B_{TCR} < 700 molecules/μm^2 (*red circles*) or the presence of high amounts of the L3-12 TCR, B_{TCR} > 900 molecules/μm^2, (*green circles*). Prominent lamellipodia formation was reached at *p* > 0.2 and is indicated with the *dashed line* (p_{lam}). Each point represents an average value for 50-100 analyzed cells per *F*-value. Data are from six and nine independent experiments for single rCD2 and L3-12 TCR, respectively, and from ten independent experiments for the protein mixture.

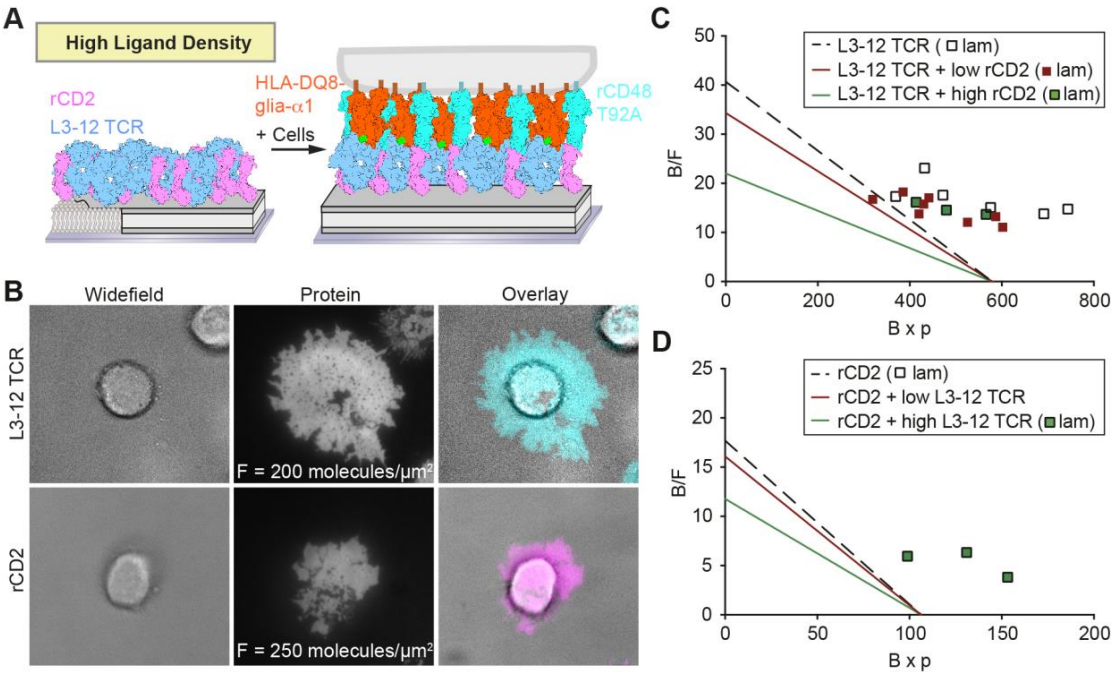

Figure 4. Lamellipodia formation coincides with a shift of the Zhu-Golan curves to the right

(A) Schematic representation of high ligand density on the SLB. **(B)** *Top panel*: Widefield image of a cell binding to L3-12 TCR, accumulated L3-12 TCR beneath that cell at high free ligand density and the merge of both. *Bottom panel*: Widefield image of a cell binding to rCD2, accumulated rCD2 beneath that cell at high *free ligand density* and the merge of both. Scale bar is 10 μm. **(C-D)** Zhu-Golan plots for (C) L3-12 TCR binding HLA-DQ8-glia-α1 ($B{\times}p$ > 300 molecules/μm^2) and (D) rCD2 binding rCD48$_{T92A}$ ($B{\times}p$ > 100 molecules/μm^2) in the presence of lamellipodia (lam). Squares represent values where lamellipodia have formed in the absence (*white*) or the presence of low (*red*) or high (*green*) amounts of the second ligand. The dashed and solid lines are linear fits to Eqn. 1 for the "low density" data as described in Figure 3. Each point represents an average value for 50-100 analyzed cells. Data are from three independent experiments.

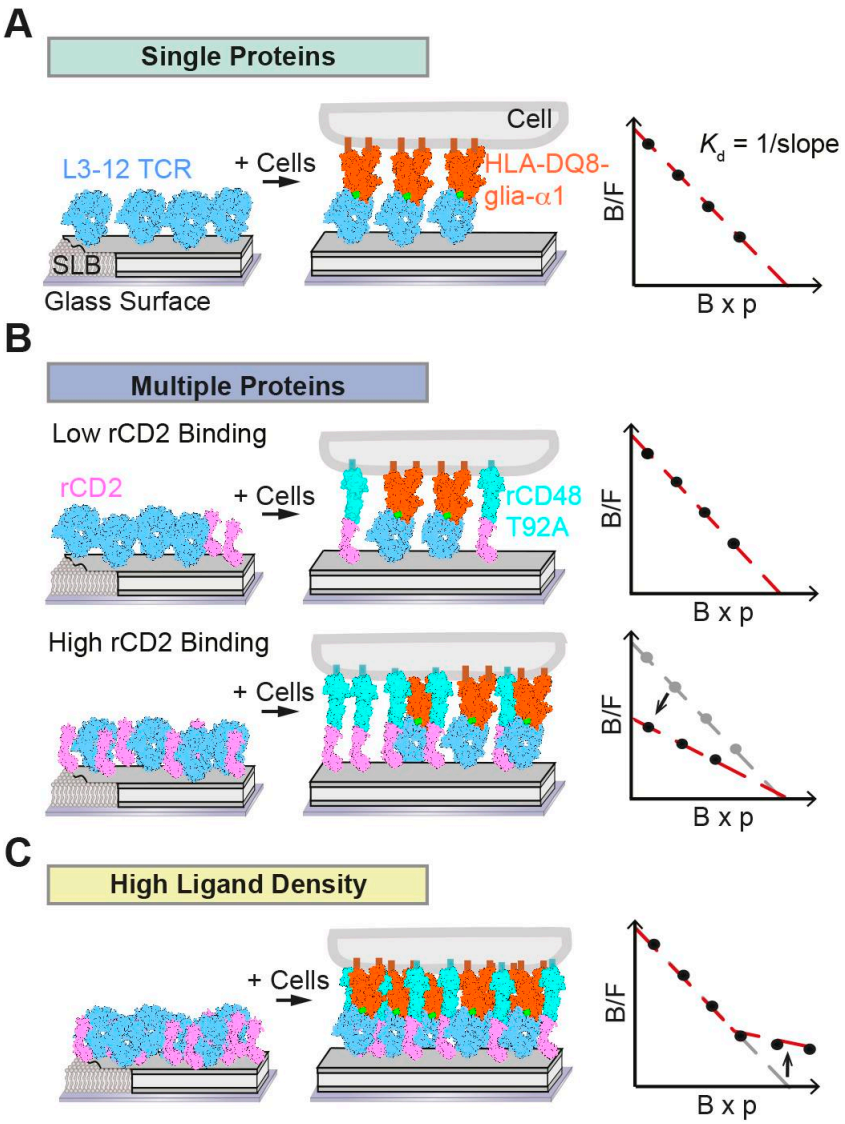

Figure 5. Measuring 2D K_ds for the ligand systems in this study using the Zhu-Golan analysis

(A) Represents the Zhu-Golan analysis to measure the 2D K_d of a specific ligand in an SLB binding to its receptor on a contacting cell (Zhu et al., 2007). The ratio between bound and free ligands, *B*/*F*, decreases when the number of bound ligands, *B*, increases, from which the 2D K_d of the interaction can be determined. **(B)** Auxiliary molecules at low densities do not affect the Zhu-Golan curve for the studied ligand-receptor interaction, however, the curve shifts downwards at higher auxiliary densities. **(C)** At high ligand densities, the cells started forming lamellipodia which coincided with a shift to the right of the Zhu-Golan curve at high *B*×*p* values.

Tables

Table 1. Parameters for L3-12 TCR binding HLA-DQ8-glia-α1 and for rCD2 binding rCD48$_{T92A}$

Ligand/ receptor[¶]	3D K_d* [μm]	2D K_d** [molecules /μm^2]	N_{tot} (Zhu-Golan) [molecules/cell]	N_{tot} (flow cytometry) [molecules/cell]	f^{π}	$D_{eff}^{\ddagger}$ [μm^2 s^{-1}]	$p_{max}^{\text{ø}}$	$B_{max}^{\text{¢}}$ [molecules/ μm^2]
L3-12 TCR/HLA -DQ8-glia-α1	7	14±5	4.5±1.2×10^5	4.5±0.1×10^5	0.9±0.1	0.3±0.05	0.38	2000
rCD2/ rCD48$_{T92A}$	11	6±1	1.2±0.1×10^5	1.1±0.1×10^5	0.8±0.2	0.6±0.13	0.15	580

[¶]The ligand is attached to an SLB and the receptors are expressed by Jurkat T cells.

*3D dissociation constant for L3-12 TCR binding HLA-DQ8-glia-α1 (Broughton et al., 2012) and rCD2 binding rCD48$_{T92A}$ (Evans et al., 2006).

**2D dissociation constant measured using the Zhu-Golan analysis in this work.

[#]Total receptor number estimated from the *x*-intercept of the Zhu-Golan plot.

[†]Total receptor number measured in flow cytometry *via* antibody labelling.

[π]Mobile fraction of receptors on the cell surface measured by FRAP.

[‡]The effective diffusion coefficient measured of the ligands in the cell-SLB contact.

[ø]Maximum average value for the ratio of the cell-SLB contact area to the total cell surface area.

[¢]Maximum number of bound ligands measured in the experiments.

Supplementary Information

Supplementary Figures

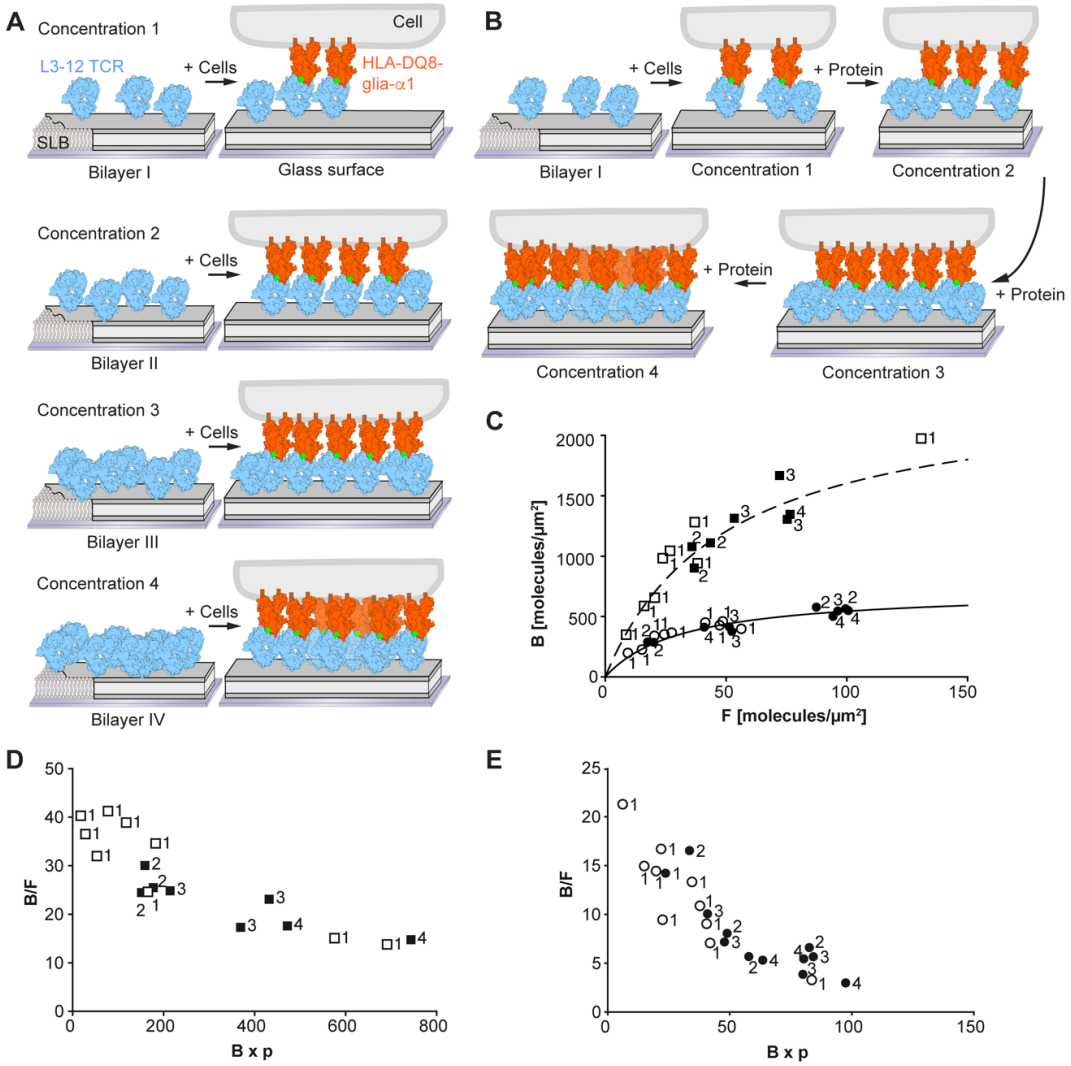

Figure S1. Comparison of Zhu-Golan analysis using multiple additions to one SLB or a different SLB for each measurement

(A) Schematic representation of four individual SLBs containing L3-12 TCR. The L3-12 TCR concentration was higher on each subsequent SLB. No further proteins were added after the cells had bound to the SLB. **(B)** Schematic representation of one SLB where increasing amounts of L3-12 TCR was added after each step. **(C)** Steady state accumulation of bound rCD2 or L3-12 TCR in the contact area as a function of free ligand density on the SLB. Data were obtained on (i) different bilayers for each experiment (*empty symbols*) or on (ii) a single bilayer and multiple additions of proteins (*black symbols*, 1 to 4 correspond to the addition number for each bilayer). **(D-E)** Zhu-Golan plots of (D) the L3-12 TCR binding HLA-DQ8-glia-α1 and (E) rCD2 binding rCD48$_{T92A}$ using both methods (i+ii). Each point represents an average value for 50-100 analysed cells per *F*-value. Data are from six (L3-12 TCR) and nine (rCD2) independent experiments.

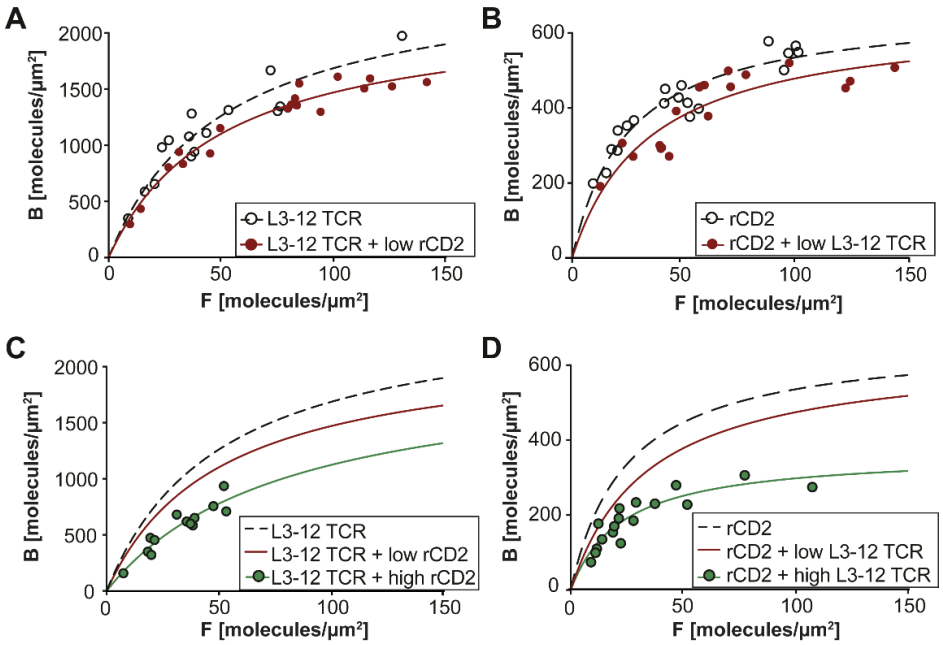

Figure S2. The amount of bound ligands vs free ligand density

(A-B) Steady state accumulation of bound (A) L3-12 TCR and/or (B) rCD2 in the contact area in presence (*red circles*) and absence *(empty circles*) of low amounts of rCD2 or low L3-12 TCR, respectively. **(C-D)** Steady state accumulation of bound (C) L3-12 TCR and (D) rCD2 in the contact area in the presence of high amounts (*green circles*) of (C) rCD2 or (D) L3-12 TCR. The *dashed lines* are fits for only one ligand on the SLB, the *red solid lines* are fits for the two-protein mixtures at low densities of auxiliary molecules and the *green solid lines* are fits of the two-protein mixtures at high auxiliary ligand densities. Each point represents an average value for 50-100 analysed cells per *F*-value. Data are from seven independent experiments.

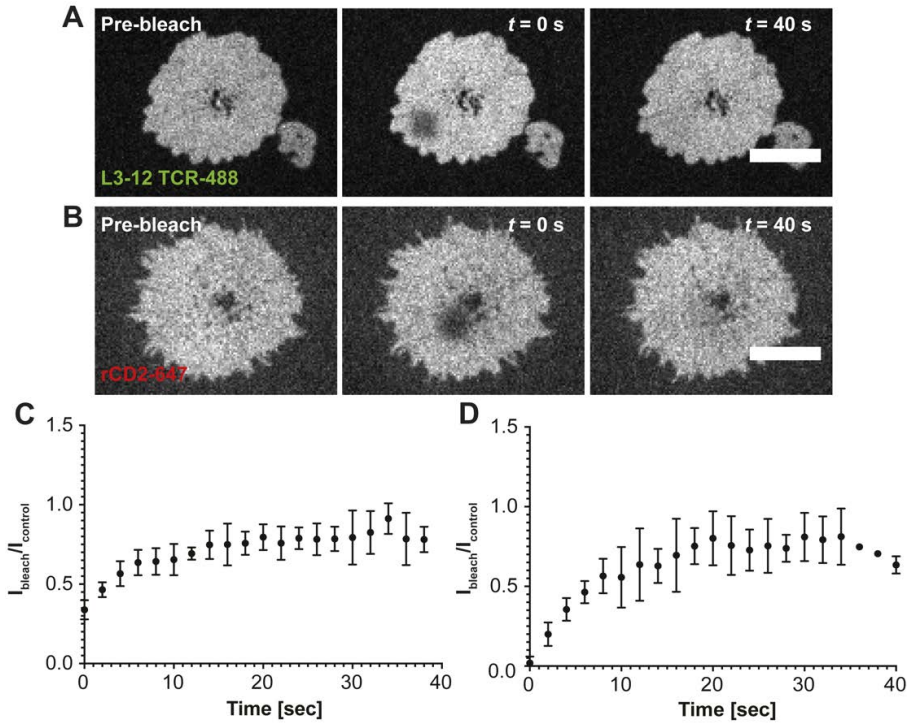

Figure S3. FRAP measurements of the ligand mobility in cell-SLB contacts

(A-B) Representative confocal images of (A) L3-12 TCR or (B) rCD2 in the contact area of a Jurkat T cell interacting with an SLB containing both proteins. Images were taken before (*Pre-bleach*) and after local bleaching (t = 0 s) as well as after recovery at t = 40 s. The scale bar is 10 µm. **(C)** Recovery curve of L3-12 TCR and **(D)** rCD2 with I_{bleach} being the intensity in the center of the bleached spot and $I_{control}$ the intensity outside the bleached spot. Data are from five different cells. Error bars is mean±s.d.

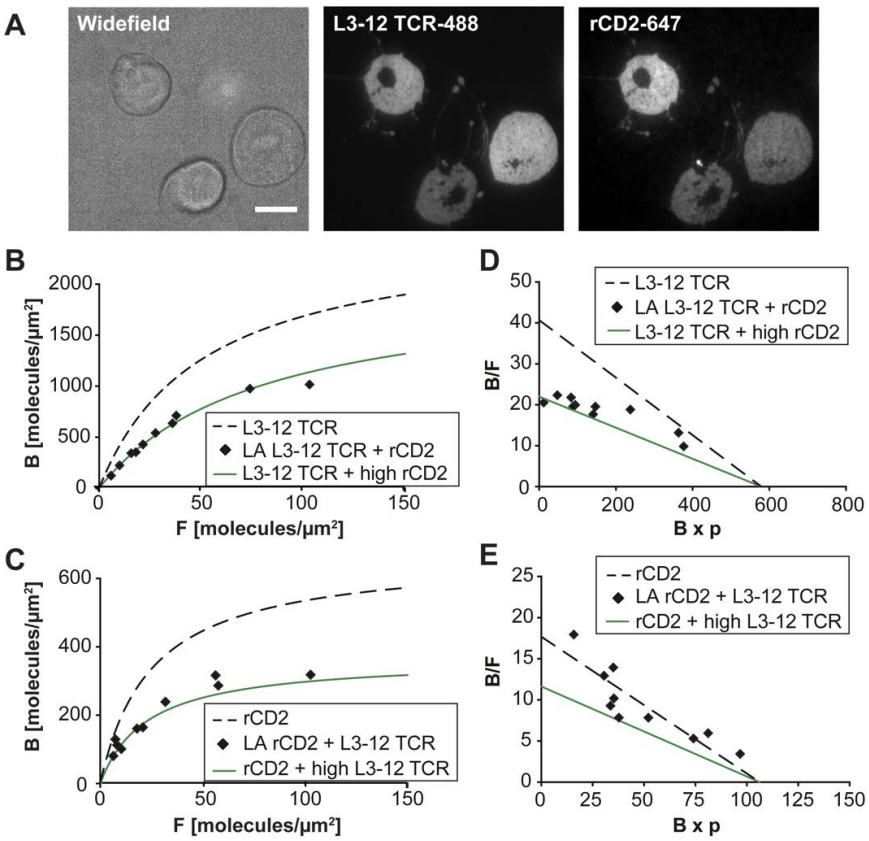

Figure S4. The effect of latrunculin A on ligand-receptor binding

(A) Images of latrunculin A treated cells. *Top panel*: Widefield image of three cells, *Middle panel*: Accumulated L3-12 TCR and *Bottom panel*: Accumulated rCD2 beneath the cells. Scale bar is 10 µm. **(B, C)** Steady state accumulation of bound (B) L3-12 TCR and (C) rCD2 beneath untreated (*dashed* and *green lines*) or latrunculin A treated cells (*black diamonds*). *Dashed lines* are for only one ligand on the SLB. *Green solid lines* are for mixtures of L3-12 TCR and rCD2 at high binding fractions of the auxiliary ligand. **(D-E)** Zhu-Golan plots for (D) L3-12 TCR binding HLA-DQ8-glia-α1 and (E) rCD2 binding $rCD48_{T92A}$ in the absence of auxiliary ligand (*dashed lines*) and for high densities of auxiliary ligands (*green solid line*) for untreated cells. *Black diamonds* are for latrunculin A treated cells on SLB containing both rCD2 and L3-12 TCR. Each point represents an average value for 30-100 analysed cells per *F*-value. Data are from three independent experiments.

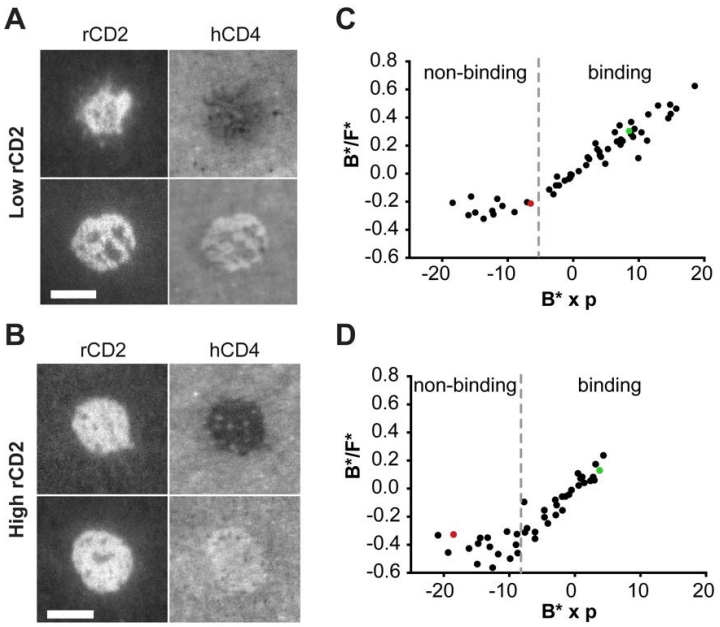

Figure S5. The influence of rCD2 density on hCD4 binding HLA-DQ8-glia-α1

(A) Images of rCD2 and hCD4 accumulation beneath different cells at low densities of bound rCD2 (B_{rCD2} = 120 ± 40 molecules/μm^2). *Top panel*: No binding of hCD4 in the contact, *Bottom panel*: Binding of hCD4 in the contact. **(B)** Images of rCD2 and hCD4 accumulation beneath different cells at high densities of bound rCD2 (B_{rCD2} = 540 ± 160 molecules/μm^2). *Top panel*: No binding of hCD4 in the contact, *Bottom panel*: Binding of hCD4 in the contact. **(C, D)** Single cell values of B^*/F^* in the presence of low (C) and high (D) densities of bound rCD2 in the cell-SLB contact (*black circles*; red/green dots correspond to the cells in the top/bottom panels in A and B). Note that B^* and F^* are not corrected for exclusion of free ligands in the cell-SLB contact. The data points to the left of the "bend" in the curves are cells not having any visible hCD4 accumulation, yielding the exclusion of free hCD4 in the cell-SLB contact, which is 25% and 41% at low and high densities of bound rCD2, respectively. The data points to the right of the "bend" are cells where hCD4 is binding. The amount of binding varies for different cells, but was on average 1.8 times lower when having high densities of bound rCD2 compared to low densities of bound rCD2.

Supplementary Movies

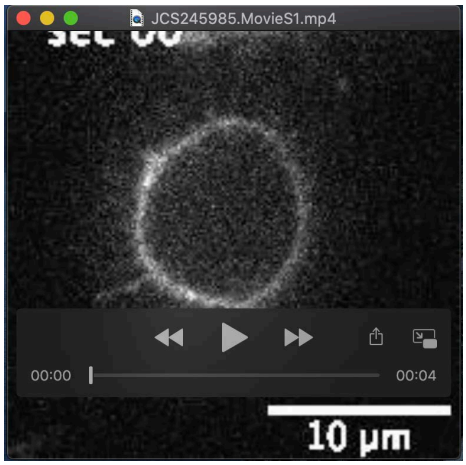

Movie 1. FRAP analysis of HLA-DQ8-glia-α1 mobility on a Jurkat T cell
Representative confocal images of HLA-DQ8-glia-α1 expressing Jurkat T cell stained with PE-anti-HLA-DQ before and after photobleaching. The bleached region is indicated with an arrow. Estimated mobile fraction, $f = 0.88$.

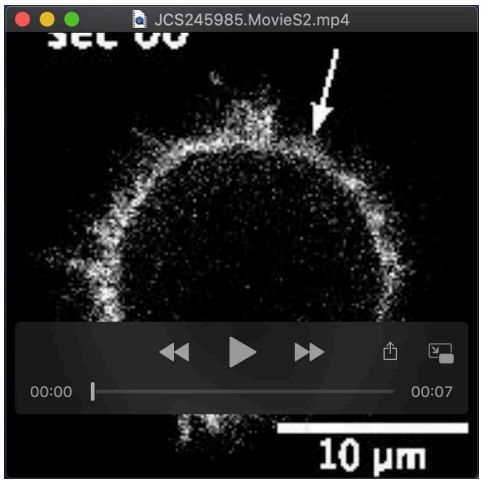

Movie 2. FRAP analysis of HLA-DQ8-glia-α1 mobility on a Jurkat T cell
Representative confocal images of HLA-DQ8-glia-α1 expressing Jurkat T cell stained with PE-anti-HLA-DQ before and after photobleaching. The bleached region is indicated with an arrow. Estimated mobile fraction, $f = 0.94$.

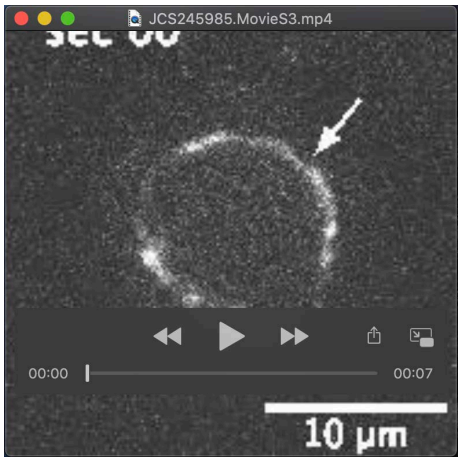

Movie 3. FRAP analysis of rCD48$_{T92A}$ mobility on a Jurkat T cell
Representative confocal images of rCD48$_{T92A}$ expressing Jurkat T cell stained with PE-anti-rCD48 before and after photobleaching. The bleached region is indicated with an arrow. Estimated mobile fraction, $f = 0.62$.

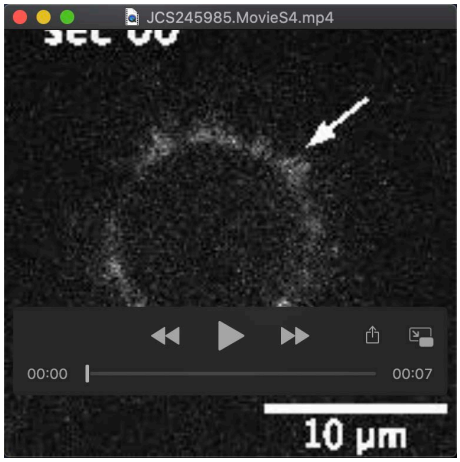

Movie 4. FRAP analysis of rCD48$_{T92A}$ mobility on a Jurkat T cell
Representative confocal images of rCD48$_{T92A}$ expressing Jurkat T cell stained with PE-anti-rCD48 before and after photobleaching. The bleached region is indicated with an arrow. Estimated mobile fraction, $f = 0.47$.

Journal of Cell Science • Supplementary information

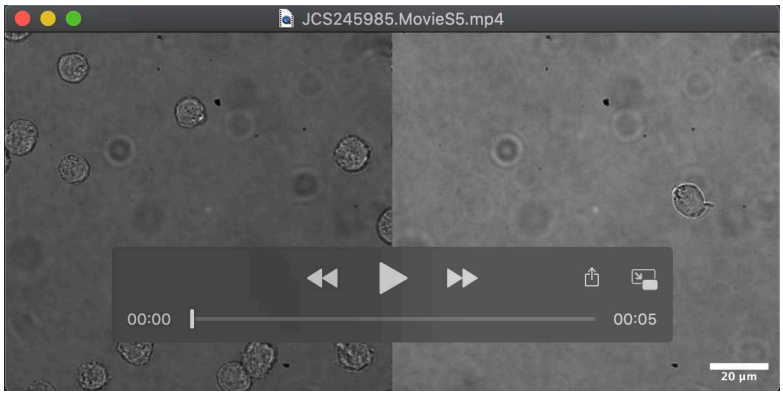

Movie 5. Binding of Jurkat T cells in media to ligand free SLBs
Representative bright field images of Jurkat T cells in supplemented RPMI media containing 10% FBS on ligand free 10% DGS-NTA SLBs before and after washing with HBS buffer.